Removal of sulfanilamide by tailor-made magnetic metal-ceramic nanocomposite adsorbents

REMOVAL OF SULFANILAMIDE BY TAILOR-MADE MAGNETIC METAL-CERAMIC NANOCOMPOSITE ADSORBENTS

Filomena Sannino[1], Michele Pansini[2], Antonello Marocco[2], Alessia Cinquegrana[3], Serena Esposito[4], Olimpia Tammaro[4], Gabriele Barrera[5], Paola Tiberto[5], Paolo Allia[4, 5], Domenico Pirozzi[3]

[1]University of Naples "Federico II", Department of Agricultural Sciences, Via Università 100, 80055 Portici (Naples, Italy)
[2]Department of Civil and Mechanical Engineering and INSTM Research Unit, Università degli Studi di Cassino e del Lazio Meridionale, Via G. Di Biasio 43, 03043 Cassino, FR, Italy
[3]University of Naples "Federico II", Department of Chemical Engineering, Materials and Industrial Production (DICMaPI), Laboratory of Biochemical Engineering. Piazzale Tecchio, 80, 80125, Naples (Italy)
[4] Department of Applied Science and Technology and INSTM Unit of Torino – Politecnico, Politecnico di Torino, Corso Duca degli Abruzzi 24, 10129, Torino, Italy.
[5]INRiM Torino, Advanced Materials for Metrology and Life Sciences, Strada delle Cacce 91, 10143 Torino, Italy

Corresponding author:

Prof. Domenico Pirozzi dpirozzi@unina.it
Department of Chemical, Materials and Production Engineering (DICMAPI)
Università di Napoli "Federico II
Piazzale Tecchio 80, 80125 Napoli, Italy
Phone: +390817682274.

Abstract

Three tailor-made magnetic metal-ceramic nanocomposites, obtained from zeolite A (ZA1 and ZA2) and a natural clinoptilolite (LB1), have been used as adsorbents to remove sulfanilamide (SA), a sulfonamide antibiotic of common use, from water.

A patented process for the synthesis of nanocomposites has been suitably modified to maximize the efficiency of the SA removal, as well as to extend the applicability of the materials.

The role played by the main process parameters (kinetic, pH, initial concentration of SA) has been characterized. The significant effect of the pH on the SA removal has been explained identifying two possibly coexisting mechanisms of SA adsorption, based on polar and hydrophobic interactions, respectively.

The adsorption kinetics have been in all cases described by the pseudo second-order model. The adsorption isotherms obtained with ZA1 have been satisfactorily described by the Langmuir model, suggesting a monolayer adsorption of SA on the magnetic nanocomposites resulting from a uniform surface energy. The isotherms obtained with LB1 could be described by a more complex approach, deriving by the additive superposition of Langmuir and Sips models.

In order to ensure an effective removal of the antibiotic and a proper recycle of the magnetic adsorbents, a sustainable regeneration procedure of the exhausted adsorbent has been developed, based on the treatment with a dilute solution of NaOH.

Key words: wastewater remediation, magnetic metal ceramic nanocomposites, antibiotic removal, sustainable regeneration

1. Introduction

The diffusion of sulfonamides (sulfa drugs, SAs) is widespread, as they are synthetic antibiotics able to inhibit both gram-positive and gram-negative bacteria. They are systematically used to treat/prevent bacterial infections (van Mil, 2011). In particular, sulfonamides antibiotics (SAs) are commonly used in human therapy, livestock production and aquaculture due to their low cost and good effect since they present a broad spectrum against Gram (+) and Gram (-) bacteria (Dibner and Richards, 2005; Neu and Gootz, 1996, Yang et al., 2016).

Unfortunately, the spread of sulfonamides is raising significant concerns as regards the public health, for different reasons:

- Sulfonamides can deteriorate the quality of drinking water and may cause potential hazard (carcinogenicity, teratogenicity and mutagenicity) because of the similarity of these compounds and the carcinogenic substances of the aniline-dye group (Qin et al., 2020).
- The resistance of Sulfonamides is widespread in many species of bacteria (Sköld, 2000).
- Sulfonamides containing the arylamine group in the position N4, such as sulfamethoxazole, sulfasalazine, sulfadiazine, and the anti-retrovirals amprenavir and fosamprenavir, may cause significant allergic responses (Giles et al., 2019). In facts, about 3% of the population have adverse reactions when treated with sulfonamide antimicrobials (Tilles, 2001).

Recently, antibiotics have been detected in natural waters at concentration levels going from 37,000 ng/L in tributaries of rivers and seas to several micrograms per liter (Sabri et al., 2020; Zhou et al., 2019; Conde-Cid et al., 2021; Dekhi-Bemani et al., 2021). For this reason they have been declared as priority substances in water protection policies (Directive 2013/39/EU).

Several technologies have been developed to remove these contaminants such as coagulation, sedimentation, advanced oxidation processes, filtration, membrane technologies, and biological treatments (Ortiz et al., 2015; Kassinos et al., 2011; Pirozzi et al., 2020; Sannino et al., 2014; Sannino et al., 2015).

However, some of these methods require additional chemicals or high amounts of energy during the process and generate wastes and byproducts that have to be disposed in subsequent steps. Reverse osmosis, ion exchange, and advanced oxidation processes, though being more attractive, do not seem to be economically feasible because of their relatively high investment and operational cost (Rashed, 2013).

Adsorption is considered an excellent process for treating wastewater containing low concentration of antibiotics, on account of the fact that it exhibits the aforementioned drawbacks to

a decidedly lower extent than the other processes. (Srivastava et al., 2009; De Gisi et al., 2016; Sannino et al., 2013a; Addorisio et al., 2011). Some previous studies have focused on the study of porous materials as adsorbents for sulfonamides (Mendiola-Alvarez et al., 2020, Conde et al., 2021).

A point of weakness of the adsorption procedures, still limiting their full application, stems from the separation of the exhausted adsorbent from water, generally obtained by centrifugation or filtration, as these methods require costly instrumentation. These procedures cannot be proposed at an industrial level, and such consideration suggested us to develop magnetic metal-ceramic nano-composites as adsorbents, that could be easily separated from the aqueous phase by the action of an external magnetic field.

In this view, tailor-made magnetic nano-composites have been produced starting from a zeolite precursor, to exploit the peculiar properties of zeolites, such as high cation exchange capacity, swelling, and wide availability. Zeolites have already been used to remove antibiotics (Sousa et al., 2018) and in particular to remove SAs from wastewaters (Blasioli et al., 2014, Martucci et al. 2014, Braschi et al., 2016), though in a non-magnetic form.

In order to obtain magnetic nano-composite adsorbents, a patented process (Esposito et al., 2014, 2015; Marocco et al., 2012; Ronchetti et al., 2010; Esposito et al., 2018) has been suitably modified. Through such a patented process (described in detail in the Materials and Method section) the final products are obtained by thermal treatment under reducing atmosphere of commercial zeolites (precursors) loaded with Fe^{2+} ions. During the thermal treatment (500-850 °C), the starting zeolite structure is almost totally degraded, and the final product of the process is a nanocomposite ceramic material that contains Fe^{0} metallic nanoparticles (NPs) evenly dispersed in a mostly amorphous silica and alumina matrix.

These materials exhibit magnetic properties (Barrera et al., 2018, 2019, 2020) owing to the presence therein of Fe^{0} ferromagnetic nanoparticles deriving from Fe^{2+} reduction. They are devoid of many features of the parent zeolite from which they originated, though they exhibit an irregular residual porosity (Esposito et al., 2018), associated to the starting zeolite precursor. These materials could be exploited for many applications such as the separation of DNA from crude cell lysate (Pansini et al., 2017) and from human blood (Esposito et al., 2020), the removal of agrochemicals from water (Pansini et al., 2018; Marocco et al., 2020) and as moon dust simulant (Freyria et al., 2019; Manzoli et al., 2021).

As it is evident from the short description of the smart and scalable process used, the proposed technique of production of magnetic nanocomposites is very simple and cheap. It is worth observing that various types of magnetic composites have been so far synthesized, most of them

obtained providing a magnetite core to an adsorbent material (Bao et al., 2014). Alternatively, magnetic adsorbents have been obtained employing iron sludge (Wan et al., 2020) or by modification of activated carbon (Guo et al., 2018). As far as we know, no magnetic materials have been so far obtained by exchange of Fe^{2+} ions.

In order to maximize the efficiency of the SA removal from water by the magnetic composites, the zeolite A and a natural clinoptilolite have been selected as starting materials. In particular, the choice of A zeolites has been dictated by their high cation exchange capacity, due to their Si/Al ratio = 1.00 (Pansini et al., 2010; Manzoli et al., 2021). As regards the clinoptilolite, its high ratio Si/Al = 4.14 (Manzoli et al., 2021) can promote hydrophobic interactions with the aromatic ring of SA.

These zeolites have been chosen also on the basis of the knowledge of their features and on the basis of their large availability with consequent relatively low cost. As a matter of facts, zeolite A is the most common synthetic zeolite in the world, whereas the powder-like clinoptilolite bearing material from Northern Sardinia is a waste, derived from cutting operations of dimension stones (Pansini et. al., 2010).

Moreover, synthetic zeolite A in its original Na form and the natural sardinian Epiclastite containing clinoptilolite have already been used in several industrial applications (Colella et al., 1998; Pansini and Colella, 1990; Albino et al., 1995; Colella and Pansini, 1988; Cioffi et al., 1996, Pansini et al., 2010; de' Gennaro et al., 2008, Basile et al., 1992).

In order to enable a sustainable industrial application of the methods developed, two main targets will be pursued:

i) to evaluate the adsorption ability of the magnetic nanocomposites in the removal of sulfanilamide antibiotic (SA) from waters by investigating the role played by the main process parameters (pH, time, initial concentration of SA);

ii) to develop a sustainable regeneration procedure of the exhausted adsorbent, to achieve proper disposal of the antibiotic and reuse of the magnetic nanocomposites with minimum energy consumption, requirement of chemicals, waste disposal.

2. Materials and methods

2.1. Materials

Reagent grade *p*-aminobenzenesulfonamide (Sulfanilamide) was obtained from Sigma-Aldrich Chemical Company (> 99.0% purity). The acetonitrile used for analytical determinations

was Carlo Erba HPLC grade. Cation exchange solutions were prepared by dissolving the proper amounts of NH_4Cl (Aldrich, 99.5 wt %) and/or $FeSO_4 \cdot 7H_2O$ (Aldrich, 99.5 wt %) in doubly distilled water.

Three magnetic metal-ceramic nanocomposites were prepared:

- ZA1 (labeled as (Fe,H)A800C-0min in previous works) and ZA2 (labeled as (Fe,H)A600C-90min in previous works) were prepared starting from Zeolite A (LTA framework type, (Baerlocher et al., 2011), $Na_{12}Al_{12}Si_{12}O_{48} \cdot 27H_2O$) Sigma-Aldrich Chemical Company;
- LB1 (labeled as SMA-LacBen in previous works) was prepared starting from a naturally occurring, clinoptilolite (HEU framework type, Baerlocher et al., 2011) bearing rock, named LacBen for the sake of uniformity with previous works (Manzoli, 2021), which comes from a deposit sited in Bortivuile (Sassari, Northern Sardinia) (Cappelletti et al. 1999; Cerri et al. 2001; Cerri et al. 2002; Langella et al. 2003;).

2.2. Preparation and characterization of materials

The preparation of magnetic metal-ceramic nanocomposites ZA1, ZA2 and LB1 was carried out following the procedures that are described in detail in the Supporting Information file (paragraph S.1).

The ζ-potential curve of samples ZA1, ZA2 and LB1 in deionized water was obtained by measuring the electrophoretic mobility as a function of pH at 25 °C by means of electrophoretic light scattering (ELS) (Zetasizer Nano-ZS, ZEN5600, Malvern Instruments, Worcestershire, UK). Suspensions were obtained after 2 min of sonication with an ultrasonic probe (100 W, 20 kHz, Sonoplus; Bandelin, Berlin, Germany); the pH of the suspension was adjusted by adding either 0.1M HCl or 0.1M NaOH (Pansini et al., 2018).

The SA was subjected to simultaneous differential thermal (DTA) and thermogravimetric analysis (TGA) under inert atmosphere (N_2), using a Perkin-Elmer thermo-analyzer STA 6000, with Al_2O_3 as reference material. The TG and DTA tests were performed keeping 9.45 mg of SA under nitrogen atmosphere, varying the temperature from 30 to 1000 °C. A heating rate of 10 °C min^{-1} was adopted.

The compositional, morphologic, textural and magnetic features of the magnetic adsorbents ZA1, ZA2 and LB, already shown in previous works (Dell'Agli et al., 2000; Clayden et al., 2003; Marocco et al., 2011; Esposito et al., 2015; Pansini et al., 2017; Pansini et al., 2018; Esposito et al., 2018; Manzoli et al., 2021) are reported in the Supporting Information file (paragraph S.2).

2.3. Analytical determination of sulfanilamide

The SA concentration in solution was analyzed with an Agilent 1200 Series HPLC apparatus (Wilmington U.S.A.), equipped with a DAD array and a Chem Station Agilent Software. A Macharey-Nagel Nucleosil 100-5 C18 column (stainless steel 250 × 4 mm) was utilized. The mobile phase, a binary system of 80:20 acetonitrile: phosphate buffer (0.1% pH 2.70), was pumped at 1 mL min^{-1} flow in an isocratic mode. The detector was set at 224 nm and injection volume was 20 μL. The quantitative determination of the antibiotic was performed using a calibration curve between 1.0–1163 μmol/L.

2.4. Adsorption experiments

100 mg of SA were dissolved in 500 mL of ultrapure water. The resulting 200 mg/L (corresponding to 1163 μmol/L) solution was kept refrigerated at 4 °C and used to prepare all solutions tested within this work. Batch experiments of SA removal from waters by adsorption on the nanocomposites ZA1, ZA2 and LB1 were performed. Aqueous solutions of SA were contacted with magnetic nanocomposites in glass vials with Teflon caps at 25 °C; the vessels were continuously stirred in an orbital shaker at speed of 150 rpm (942 rad/min). At fixed times, the magnetic adsorbents were separated from the liquid using an external magnet (VA03, UNIDISP s.r.l. Italy) and the liquid was analysed to evaluate SA concentration by HPLC analysis. The amount of SA adsorbed was calculated as the difference between its initial and final concentration in solution. Blanks of SA in ultrapure water were analysed in order to evaluate SA stability and sorption on vials. The following experimental factors were evaluated:

(a) Effect of pH: samples of magnetic nanocomposites ZA1, ZA2 and LB1 were contacted with 40.0 μmol/L SA solution at solid/liquid ratio (S/L) = 1/10,000 g/g for 24 h (this time was shown to be sufficient to attain an equilibrium condition). The pH of this solution varied between 2.0 and 8.0, in steps of 0.5, by adding the proper amount of 0.01 or 0.10 mmol/L HCl or NaOH aqueous solution.

(b): Adsorption kinetics - These tests were performed using the two magnetic adsorbents which exhibit the best results (ZA1 and LB1) at the pH of maximum adsorption (6.0 and 4.0, respectively), as discussed in the paragraph 3.2. Samples of ZA1 and LB1 were contacted with 40.0 or 126 μmol/L SA solutions, at solid/liquid ratio S/L = 1/10,000 g/g at pH 4.0 for LB1 and pH 6.0 for ZA1. The suspensions were stirred for 10, 30, 60, 120, 240, 360, 900 and 1440 min and successively subjected to the separation procedure described

(c) Adsorption isotherm – The magnetic adsorbents ZA1 and LB1 were contacted with solutions having SA concentration up to 1163 μmol/L at S/L = 1/10,000 g/g, T = 25 °C and pH = 6.0 or 4.0, respectively, for 24 h. The pH of each suspension was kept constant by adding proper amounts of 0.01 or 0.10 mmol/L HCl or NaOH solution.

2.5. Desorption and recycle experiments

The desorption and reuse experiments were carried out following two different approaches, namely thermal desorption and alkali desorption.

In both cases, ZA1 and LB1 magnetic adsorbents were preliminarily used to adsorb SA at the initial concentration of 40 μmol/L for 24 h.

The thermal desorption was carried out incubating the exhausted samples of ZA1 and LB1 bearing adsorbed sulfanilamide at 400 °C for 10 min under inert nitrogen atmosphere. Thus, the adsorbents were magnetically separated, and their adsorption capacity tested with a fresh solution of sulfanilamide.

In the alkali desorption, the exhausted samples of ZA1 and LB1 were put in contact with a NaOH solution for a fixed time at constant temperature. Thus, the adsorbents were magnetically separated, and the concentration of the desorbed SA in the liquid phase was determined.

In both cases, new adsorption tests were carried out to measure the efficiency of the regenerated adsorbents, incubating the magnetic adsorbents for 24 h in a SA solution at the initial concentration of 40 μmol/L for 24 h.

2.6. Statistical analysis

All data are presented as mean ± standard deviation (n = 3). SPSS program (version 20) was used for analyzing and the statistical significant ($P < 0.05$) was determined using Student's t-test.

3. Results and Discussion

3.1. Textural and morphological characterization of the magnetic nanocomposites

During the thermal treatments under reducing atmosphere, Fe-exchanged zeolites are known to undergo the following phenomena (Breck,1974, Dwyer, 1989; Colantuono et al., 1997): (i) shrinkage by dehydration, (ii) reduction to Fe^0 (with a possible structural damage of the zeolite framework), (iii) migration of the newly formed Fe^0 atoms to form clusters located within the

microporous cavities of the zeolite, (iv) migration of the newly formed Fe^0 atoms outside the ze3olite cavities to form metallic particles at the outer surface of the zeolite grains, (v) thermal collapse of the zeolite framework, (vi) possible formation of amorphous and other crystalline phases.

Thus, changing the starting material and the conditions of the thermal treatment under reducing atmosphere may give rise to largely different final products. In particular, the different thermal treatment of the different starting materials (accurately described in the supporting informations) resulted in the formation of the magnetic adsorbents ZA1, ZA2 and LB1. The Figure S1 reports their SEM images, whereas the Table S1 reports their quantitative phase determinations, textural and magnetic properties. These measurements revealed the existence of magnetic Fe^0 nanoparticles with size is in the 5-30 nm range, together with a residual fraction of Fe cations still dissolved in a prevailingly amorphous ceramic phase. This phase is originated from the thermal collapse of the microporous zeolite structure, as confirmed by the textural data.

The overall magnetic response at room temperature was found to be dominated by Fe^0 and/or Fe oxide nanoparticles giving a high magnetic saturation and a coercivity of the order of 300-500 Oe, typical of blocked magnetic nanoparticles, together with a small unsaturating contribution from the few Fe cations still dissolved in the matrix. When the material is submitted to a non-uniform magnetic field with a strength typical of laboratory permanent magnets, Fe-exchanged zeolites are able to generate – after structural collapse - a magnetic force sufficient to guarantee the magnetic separation of the solid adsorbent from the liquid (Esposito et al., 2020; Pansini et al., 2018; Freyria et al., 2019).

The overall magnetization (per gram of material) of these magnetic metal-ceramic nanocomposites depends on both the intrinsic nanoparticle magnetization and on the volume density of particles generated during thermal treatment. As a matter of fact, the overall magnetization of samples ZA1 and ZA2 turns out to be significantly larger than the one of sample LB1, as shown in Table S1. In the latter case, the low magnetization value directly depends on the lower resulting concentration of Fe^0 particles (Table S1); in the two nanocomposites obtained from zeolite A (ZA1, ZA2), a lower-temperature treatment for a longer time gives the best result. Another important parameter influencing the performance of these nanocomposites in magnetic separation is the maximum magnetic susceptibility, roughly corresponding to the slope of the M(H) curve, which gives information about the minimum field needed to actuate the magnetic separation process. This parameter is much larger (by a value of the order of 100) in ZA1 and ZA2 obtained from zeolite A than in LB1.

3.2. Effect of pH

The Figure 1 reports the amount of SA adsorbed on ZA1, ZA2 and LB1 magnetic adsorbents at S/L ratio = 1/10,000 after a contact of 24 h, as a function of pH. The adsorption capacity of all the magnetic adsorbents tested was strongly dependent on pH: sharp maximums were recorded at pH 6.0, 7.0 and 4.0 for ZA1, ZA2 and LB1, respectively, and small deviations from these values resulted in a marked SA adsorption decrease.

In order to explain why the SA adsorption is highly dependent on the pH, it should be taken into account that pH affects the surface charge distribution of both the antibiotic and the magnetic adsorbents.

As far as concerns to the antibiotic, the pH-dependent SA structure, similarly to other sulfa drugs, undergoes two acid-base processes (Boreen et al., 2004; Fukahori et al., 2013), due to the protonation and the deprotonation of the amino and sulfonamide groups, as shown in the Figure 2(a). The protonation state of SA can therefore be described by two values of pK (Braschi et al., 2013; Uhlemann et al, 2021): $pK_1 = 1.78$, $pK_2 = 10.6$. From these values, it is possible to obtain the speciation of SA as a function of pH (Dai et al., 2017), as shown in the Figure 2(b). These data suggest that in the range of pH 4.0-8.0 most of SA molecules are in their neutral form.

As far as concerns to the magnetic adsorbents, we measured their ζ-potential for pH varying from 1.5 to 10, as reported in the Figure 3. From these results it was possible to calculate the point of zero potential (PZC) for all the adsorbents tested: in particular, the adsorbents ZA1 and ZA2, though both obtained from the zeolite A which has Si/Al = 1.00 (Baerlocher et al., 2001), showed different values of PZC: ~4 for ZA1 and ~6 for ZA2. The adsorbent LB1 is derived from a natural high-silica clinoptilolite, with a ratio Si/Al = 4.14 (Manzoli et al., 2021), and consequently shows a more acidic behaviour, with a PZC value of about 1.4.

Putting together all these results, we can discuss the adsorption behaviour of each adsorbent. Let us start from LB1:

- when pH < 1.4, the adsorption power is prevented by the electrostatic repulsion between LB1 and SA, as they are both positively charged (Figures 2(b) and 3, respectively)
- conversely, when pH > 8.0, LB1 and SA are both negatively charged (Figures 2(b) and 3); again, the adsorption power is prevented by the electrostatic repulsion.

In the pH range from 1.4 to 8.0, two mechanisms can be hypothesized for the adsorption of SA by the adsorbent LB1:

(i) the acidic silanol groups on the surfaces of LB1 may form hydrogen bonds with the lone pair electrons of nitrogen atoms contained in the basic amino group of the SA molecules. A similar mechanism has been hypothesized in previous studies (Sannino et al., 2012; Marocco et al., 2011;

Sannino et al, 2013b; Esposito et al., 2013) concerning the use of different adsorbents such as zeolite H-Y or porous silica to remove simazine, another compound containing nitrogen atoms with lone pair electrons. It is interesting to note that this reaction cannot occur at very acidic pH values (where hydronium cations preferentially react with the lone pair electrons of nitrogen atoms of the amino groups of SA, forming substituted species that prevent the adsorption process), as well as at very alkaline pH values (where hydroxyl anions, which are stronger bases compared to the amino and sulfonamide groups on the SA, preferentially react with the hydrogen atoms of silanols, preventing the adsorption of SA).

(ii) in a previous work, Fukahori and coworkers (2013) made the hypothesis that hydrophobic interactions may occur between the aromatic ring of SA molecules and the surfaces of the adsorbents.

As already observed, the optimal value of pH for SA adsorption on LB1 was about 4.0. From the Figure 2(b) it can be seen that at pH 4.0 the prevailing form of SA is electrically neutral. On the other hand, the Figure 3 shows that charge of the adsorbent LB1 is moderately negative. Yet, the adsorbent LB1, due to its high content of silica, exhibits a hydrophobic character. Consequently, both the mechanisms (i) and (ii) are possible, and may coexist.

It is interesting to note that, in some cases described in the Literature (Al-Ghouti et al., 2020), competing cations contained in wastewaters can be exchanged with cations included in the zeolite structure, thus reducing the affinity between zeolite and adsorbate. Obviously, when using LB1 to adsorb SA, if hydrophobic interactions play a significant role in the interaction (as hypothesized by Fukahori et al., 2013), such negative effect of competing cations would be negligible.

Similar considerations can be drawn as regards the adsorption of SA on the magnetic adsorbents ZA1 and ZA2.

As observed previously, the adsorbents ZA1 and ZA2 are characterized by higher values of the point of zero charge (Figure 3): PZC~1.4 for LB1, PZC~4 for ZA1, and PZC~6 for ZA2. A similar trend can be observed in the pH values at which the maximum adsorption occurs: pHmax~4.0 for LB1, pHmax~6.0 for ZA1 and pHmax~7.0 for ZA2.

The higher concentration of silanols in the adsorbent LB1, compared to those of ZA1 and ZA2, leads to its higher SA adsorption ($9.80 \cdot x\ 10^4$ µmol/kg for LB1, $7.00\ x \cdot 10^4$ µmol/kg for ZA1, $6.00\ x \cdot 10^4$ µmol/kg for ZA2), for two reasons. First, silanol groups are directly involved in the mechanism (i). Secondarily, the higher concentration of siloxane groups (generated by silanol hydration during the thermal treatment) causes higher hydrophobicity, thus promoting the mechanism (ii).

The two magnetic adsorbents (ZA1 and LB1) which exhibited the best results in terms of amount of adsorbed SA at the pH of maximum adsorption (6.0 and 4.0, respectively) were selected for the subsequent experiments.

3.3. Kinetic and equilibrium features of the adsorption process

The Figure 4a reports the SA uptake by ZA1 and LB1 magnetic adsorbents (S/L ratio = 1/10,000, pH 6.0 and 4.0, respectively) from an aqueous solution exhibiting an initial SA concentration of 40.0 μmol/L, as a function of time. Both curves show that the uptake is initially quite rapid, then gradually slows down and attains an equilibrium condition after about 360 min.

The Figure 4b reports SA uptake from water by LB1 magnetic adsorbent (S/L ratio = 1/10,000, pH 4.0) from SA solutions of initial concentration of 40.0 and 126 μmol/L, as a function of time. Clearly, higher equilibrium values of SA uptake are attained as higher initial concentrations of SA solution are adopted. The contact time of 360 min is sufficient to attain an equilibrium condition also for the solution of initial SA concentration of 126 μmol/L. Consequently, the values of SA uptake or residual concentration in solution recorded under such circumstances were considered as equilibrium values in further elaborations.

The best model describing the adsorption kinetics reported in Fig. 4a and 4b is the pseudo second-order model, which can be expressed in a linear form according to Eq. (1) (Ozacar and Sengil, 2006):

$$\frac{t}{q} = \frac{1}{k_2 \cdot q_e^2} + \frac{t}{q_e}$$

where q_e and q are the amount of SA adsorbed (μmol/kg) at equilibrium and at time t, respectively, k_2 is the rate constant of adsorption (kg/μmol min) and t is the time (min). The values of parameters calculated for two different concentrations of SA by using LB1 are as follows. For 40 μmol/L of SA: q_e = (1.05 ± 0.01) *x* 10^5 μmol/kg, k_2 = 0.018 ± 0.002 (kg/μmol min), r^2 = 0.99; for 126 μmol/L of SA: q_e = (1.73 ± 0.12) *x*·10^5 μmol/kg, k_2 = 0.057 ± 0.001 (kg/μmol min), r^2 = 0.99. As regard ZA1 the following kinetic parameters were evaluated for 40 μmol/L concentration of SA: q_e = (7.77 ± 0.88) *x* 10^4 μmol/kg, k_2 = 0.041 ± 0.001 (kg/μmol min), r^2 = 0.99.

The Figure 5 reports the isotherms for both the ZA1 and LB1 magnetic adsorbents. A regression analysis showed that the more suitable model to describe the isotherm obtained with ZA1

is the Langmuir model, so indicating the monolayer adsorption of SA on the magnetic nanocomposites resulting from a uniform surface energy:

$$q_e = \frac{Q_0 \cdot C_e}{\frac{1}{b} + C_e}$$

where C_e is the equilibrium concentration (μmol/L), and q_e is the amount of SA adsorbed per kilogram at equilibrium (μmol/kg). Q_0 and b are Langmuir constants related to the adsorption capacity (μmol/kg) and energy of adsorption (L/μmol), respectively.

The values of Q_0 and b obtained by nonlinear interpolation are $(4.97 \pm 0.07)\ x\ 10^5$ (μmol/kg) and $(5.62 \pm 0.01)\ x\ 10^{-3}$ (L/μmol), respectively.

The isotherm obtained with LB1, showing a more complex behaviour, can be considered a type IV isotherm. The best model to describe this isotherm was obtained by the additive superposition of the models of Langmuir and Sips (Buttersack, 2019), yielding the following mathematical expression:

$$q_e = Q_0 \cdot \left(\frac{C_e}{\frac{1}{b'} + C_e} + \frac{C_e^5}{\frac{1}{b''} + C_e^5} \right)$$

where the meaning of the variables C_e, q_e, and of the parameter Q_0 is unchanged. The parameter b' is the energy of adsorption (L/μmol), whereas b'' is a parameter of the model of Sips ($L^5/\mu mol^5$). The values of Q_0, b' and b'' obtained by nonlinear interpolation are $(4.41 \pm 0.06)\ x\ 10^5$ (μmol/kg), $(5.10 \pm 0.07)\ x\ 10^{-14}$ (L/μmol) and $(1.52 \pm 0.03)\ x\ 10^{-2}$ (L/μmol), respectively.

The results obtained in our investigation are promising if compared with other studies. The adsorption capacity of the adsorbent LB1, expressed as the ratio (weight SA/weight LB1), is substantially consistent or better in comparison to other studies in the Literature, concerning the sulfanilamide removal with different non-magnetic adsorbents: Fe_3O_4 nanoparticles (Dai et al., 2017), activated carbon (Korzh et al., 2016), crosslinked polystyrene (Kochuk et al, 2011). Our results were as well consistent in comparison to previous studies carried out using magnetic nanoparticles with a magnetite core (Bao et al., 2014; Shi et al., 2015; Dai et al., 2017) or obtained from iron sludge (Wan et al., 2020).

Interestingly, some of these authors (Bao et al., 2014; Dai et al., 2017; Wan et al., 2020) confirmed that the adsorption kinetics of SAs were well defined by the second-order model

Some authors (Kochuk et al, 2011; Shi et al., 2015; Dai et al., 2017; Wan et al., 2020) also found equilibrium isotherms well described by the Langmuir model, whereas Bao et al. (2014)

adopted the Dual-mode model (a combination of Langmuir equation with a linear equation), revealing that the adsorption process consisted of an initial partitioning stage and a subsequent hole-filling stage.

As regards the adsorption mechanism, Bao et al., (2014), Shi et al (2015) and Wan et al. (2020) found electrostatic interactions to be an important driving force for adsorption process. Yet, Bao et al. also underscored the effect of hydrogen bonding, whereas Wan et al. highlighted the role of hydrophobic interactions.

3.4. Thermal analysis

The SA was also characterized as regards DTA analysis (Figure 5a) and TG analysis (Figure 5b). The DTA curve exhibits an exothermic effect denoted by a sharp peak at about 180 °C and an endothermic effect, which occurs in the temperature range 280-340 °C and attains its maximum at about 320 °C. The TG curve exhibits a small weight loss of about 5 % in the temperature range room temperature-280 °C and then an evident weight loss of about 50 % in the temperature range 280-340 °C. For temperatures higher than this last value the weight of SA almost linearly decreases (with a small slope) thus attaining a final weight of about 18 % of the initial value at about 1000°C.

The DTA and TG curve of SA may be interpreted by considering that the exothermic peak at about 180 °C is due to a molecular rearrangement reaction. Such molecular rearrangement reaction results in a final product of lower enthalpy and, thus, in the release of the energy amount related to the same exothermic peak. The small weight loss in this temperature range may be reasonably ascribed to SA evaporation.

The endothermic effect, occurring in the temperature range 280-340 °C and attaining its maximum at about 320 °C, is related to the thermal decomposition of sulfanilamide molecule. This interpretation is confirmed by the TG curve, which records a mass reduction of more than 50 % in this temperature range.

3.5. Desorption and reuse of ZA1 and LB1 *magnetic adsorbents*

The results of the DTA and TG curve suggested a simple thermal regeneration method of the exhausted magnetic adsorbents. The magnetic adsorbents ZA1 and LB1 bearing adsorbed sulfanilamide was incubated at 400 °C for 10 min under inert nitrogen atmosphere. Such a thermal treatment, though not producing any structural variation in the magnetic adsorbent, yielded a full removal of the antibiotic. In facts, once the thermal treatment was completed, the sulfanilamide

uptake by the regenerated magnetic adsorbents was in all cases about 99% of the uptake obtained using the fresh material (data not shown).

In order to find a more environmentally friendly strategy, an alkali desorption procedure was also developed, based on the incubation of exhausted samples of ZA1 and LB1 in a NaOH solution. In this view, different conditions were tested in terms of incubation times, temperature and NaOH concentration. The best results were obtained carrying out the incubation in a 0.2 M NaOH solution under stirring at 25 °C for 3 h. Both ZA1 and LB1 magnetic adsorbents were subjected to three consecutive desorption-reuse cycles to evaluate the efficiency of the desorption method (Rizzi et al., 2021). The adsorption capacity of the regenerated adsorbents after each regeneration cycle are reported in the Figure 7. By a comparison between the results in the Figures 1 and 7, it can be observed that after three cycles, both the regenerated adsorbents LB1 and ZA1 kept almost entirely their adsorption capacities (95,600 μmol/kg and 50,000 μmol/kg, respectively) of their fresh counterparts.

4. Conclusions

Three tailor-made magnetic metal-ceramic nanocomposites, obtained from zeolite A (ZA1 and ZA2) and a natural clinoptilolite (LB1), have been developed by a cation-exchange treatment followed by a thermal treatment at relatively moderate temperatures under reducing atmosphere. The nanocomposites have been successfully tested as adsorbents to remove the sulfanilamide, a sulfonamide antibiotic of common use, from water.

The adsorption behaviour of the nanocomposites has been characterized, showing that the efficiency of the magnetic adsorbents strongly depends on pH. Two adsorption mechanisms, possibly coexisting, have been hypothesized taking into account the pH effects on the surface charge distribution of both the antibiotic and the magnetic adsorbents. The first mechanism is based on the formation of hydrogen bonds between silanol groups of the adsorbent and the amine group of the antibiotic, whereas the second mechanism takes into account possible hydrophobic interactions.

Two adsorbents, namely ZA1 and LB1, were then selected on the basis of their adsorption capacity, and eventually characterized as regards the adsorption kinetics. All the experimental curves were best described by the pseudo-second order model.

The equilibrium isotherms of the adsorbent ZA1 were satisfactorily described by the Langmuir model, whereas the isotherm of the adsorbent LB1 required the adoption of a more complex model, obtained by the additive superposition of the models of Langmuir and Sips.

Two procedures were developed for the regeneration of exhausted adsorbents. First, a thermal regeneration procedure was developed on the basis of the results of DT and TGA analyses, allowing the complete removal of the SA and the proper recycle of the magnetic adsorbents. Secondarily, an alkali desorption, more environmentally friendly, was carried out, again obtaining the complete regeneration of the magnetic adsorbents.

The results obtained are encouraging, demonstrating that magnetic metal-ceramic nanocomposites obtained from zeolites offer technically and economically feasible method to remove sulfonamides from aqueous solutions, ensuring environmental sustainability as well as multicycle stability and regenerability of the adsorbent materials.

Declaration of Competing Interest

The authors report no declarations of interest.

References

Addorisio V., Pirozzi D., Esposito S., Sannino F., 2011. Decontamination of waters polluted with simazine by sorption on mesoporous metal oxides. Journal of Hazardous Materials 196, 242-247. https://doi.org/10.1016/j.jhazmat.2011.09.022

Albino V., Cioffi R., Pansini M., Colella C., 1995. Disposal of lead-containing zeolite sludges in cement matrix. Environ. Technol. 16, 147-156. https://doi.org/10.1080/09593331608616255.

Al-Ghouti, M.A., Al-Absi, R.S. 2020. Mechanistic understanding of the adsorption and thermodynamic aspects of cationic methylene blue dye onto cellulosic olive stones biomass from wastewater. *Sci Rep* 10**,** 15928-15946. https://doi.org/10.1038/s41598-020-72996-3.

Baerlocher C., Meier W.M., Olson D.H., MAZ. Atlas of the zeolite framework types, Elsevier, Amsterdam, 2001.

Bao X.L., Qiang Z.M., Chang J.H., Ben W.W., Qu J.H., 2014. Synthesis of carbon-coated magnetic nanocomposite (Fe_3O_4 @C) and its application for sulfonamide antibiotics removal from water. J Environ Sci 26:962 – 969.

Barrera G., Allia P., Bonelli B., Esposito S., Freyria F.S., Pansini M., Marocco A., Confalonieri G., Arletti R., Tiberto P., 2020. Magnetic behavior of Ni nanoparticles and Ni^{2+} ions in weakly loaded zeolitic structures. J. Alloys Compd. 817, 152776-152786. https://doi.org/10.1016/j.jallcom.2019.152776 .

Barrera G., Tiberto P., Allia P., Bonelli B., Esposito S., Marocco A., Pansini M., Leterrier Y., 2019. Magnetic properties of nanocomposites. Appl. Sci. 9, 212-240. https://doi.org/10.3390/app9020212 .

Barrera G., Tiberto P., Esposito S., Marocco A., Bonelli B., Pansini M., Manzoli M., Allia P., 2018. Magnetic clustering of Ni^{2+} ions metal-ceramic nanocomposites obtained from Ni-exchanged zeolite precursors. Ceram. Int. 44, 17240-17250. https://doi.org/10.1016/j.ceramint.2018.06.182

Basile A., Cacciola G., Colella C., Mercadante L., Pansini M., 1992. Thermal conductivity of natural zeolite-PTFE composites. Heat Recover. Syst. CHP 12, 497-503. https://doi.org/10.1016/0890-4332(92)90018-D .

Blasioli S., Martucci A., Paul G., Gigli I., Cossi, Johnoston C.T., Marchese I., Braschi I., 2014. Removal of sulfamethoxazole sulfonamide antibiotic from water by high silica zeolites: A study of the involved host-guest interactions by a combined structural, spectroscopic, and computational approach. J. Coll. Interf. Sci. 419, 148-159. https://doi.org/10.1016/j.jcis.2013.12.039 .

Boreen A.L., Arnold W.A., McNeill K., 2004. Photochemical fate of sulfa drugs in the aquatic

environment: sulfa drugs containing five-membered heterocyclic groups. Environ. Sci. Technol. 38, 3933-3940. https://doi.org/10.1021/es0353053.

Braschi I., Paul G., Gatti G., Cossi M., Marchese L., 2013. Embedding monomers and dimers of sulfonamide antibiotics into high silica zeolite Y: an experimental and computational study of the tautomeric forms involved. RSC Advances 3, 7427-7437. https://doi.org/10.1039/C3RA22290J .

Braschi I., Martucci A., Blasioli S., Mzini L. L., Ciavatta C., Cossi M. (2016) Effect of humic monomers on the adsorption of sulfamethoxazole sulfonamide antibiotic into a high silica zeolite Y: An interdisciplinary study. Chemosphere 155, 444 - 452.

Breck, D.W., 1974. Zeolite Molecular Sieves: Structure, Chemistry and Uses. Wiley, New York.

Buttersack, C., 2019. Modeling of type IV and V sigmoidal adsorption isotherms. Physical chemistry chemical physics. PCCP, 21 10, 5614-5626.

Cappelletti, P.; Langella, A.; Cruciani, G., 1999. Crystal-chemistry and synchrotron Rietveld refinement of two different clinoptilolites from volcanoclastites of North-western Sardinia. Eur. J. Mineral. 11, 1051-1060.

Cerri G., Cappelletti P., Langella A., de' Gennaro M., 2001. Zeolitization of Oligo-Miocene volcaniclastic rocks from Logudoro (northern Sardinia, Italy). Contrib. Mineral. Petrol. 140(4), 404-421.

Cerri, G., Langella, A., Pansini, M., Cappelletti, P., 2002. Methods of Determining Cation Exchange Capacities for Clinoptilolite-Rich Rocks of the Logudoro Region in Northern Sardinia, Italy. Clays Clay Miner., 50 (1), 127-135.

Cioffi C., Pansini M., Caputo D., Colella C., 1996. Evaluation of mechanical and leaching properties of cement-based solidified materials encapsulating Cd-exchanged natural zeolites. Environ. Technol. 11, 1215-1224. https://doi.org/10.1080/09593331708616491 .

Clayden, N.; Esposito, E.; Ferone, C.; Pansini. M., 2003. ^{27}Al and ^{28}Si NMR study of the thermal transformation of Ba-exchanged zeolite A into monoclinic celsian. J. Mat. Chem., 13, 1681-1685.

Colantuono, A.; Dal Vecchio, S.; Mascolo, G.; Pansini, M. 1997, Thermal shrinkage of various cation forms of zeolite A. Thermochimica Acta, 296, 59-66.

Colella C., De' Gennaro M., Langella A., Pansini M., 1998. Evaluation of natural phillipsite and chabaziteas cation exchangers for copper and zinc. Sep. Sci. Technol. 33, 467-481. https://doi.org/10.1080/01496399808544991 .

Colella C., Pansini M., 1988. Lead Removal for Wastewaters Using Chabazite Tuff. ACS Symposium Series; ACS, pp. 500-510.

Conde-Cid M., Cela-Doblanca R., Ferreira-Coelho G., Fernadez-Calvino D., Nuñez-Delgado A., Fernandez-Sanjurjo M.J., Arias-Estevez M., Alvarez-Rodriguez E., 2021. Sulfadiazine, sulfamethazine and sulfachloropyridazine removal using three different porous materials: Pine bark,“oak ash” and mussel shell. Env. Res. 195. 110814-110820. https://doi.org/10.1016/j.envres.2021.110814.

Dai, K., Wang, F., Jiang, W. Chen Y., Mao J., Bao J., 2017. Magnetic Carbon Microspheres as a Reusable Adsorbent for Sulfonamide Removal from Water. Nanoscale Res. Lett. 12, 528-537. https://doi.org/10.1186/s11671-017-2295-2

de Gennaro R., Langella A., D’Amore M., Dondi M., Colella A., Cappelletti P., de’ Gennaro M., 2008. Use of zeolite-rich rocks and waste materials for the production of structural lightweight concretes. Appl. Clay Sci. 41, 61-72. https://doi.org/10.1016/j.clay.2007.09.008 .

De Gisi S., Lofrano G., Grassi M., Notarnicola M., 2016. Characteristics and adsorption capacities of low-cost sorbents for wastewater treatment: A review. SM&T 9, 10-40. https://doi.org/10.1016/j.susmat.2016.06.002 .

Dekhi-Bemani Y., Mir Leilabady N., Fu M., Rietveld L.C., van der Hoek J.P., Heyman S.G.J., 2021. Simultaneous removal of ammonium ions and sulfamethoxazole by ozone regenerated high silica zeolites. Wat. Res. 188, 116472-116481. https://doi.org/10.1016/j.watres.2020.116472

Dell'Agli, G.; Ferone, C.; Mascolo, G.; Pansini M., 2000. Crystallization of monoclinic zirconia from metastable phase. Solid State Ionics, 127, 223-230.

Dibner J.J., Richards J.D., 2005. Antibiotic growth promoters in agriculture: history and mode of action. Poult. Sci. 84, 634-643. https://doi.org/10.1093/ps/84.4.634 .

Directive 2013/39/EU of the European Parliament and of the Council of 12, Amending directives 2000/60/EC and 2008/105/EC as regards priority substances in the field of water policy. Off. J. Eur. Union L226, 2013, 1–17.

Dwyer, F.G.; 1989, An Introduction to Molecular Sieves Zeolites, J. Wiley and Sons, Chichester, UK.

Esposito S., Dell’Agli G., Marocco A., Bonelli B., Allia P., Tiberto P., Barrera G., Manzoli M., Arletti R., Pansini M., 2018. Magnetic metal-ceramic nanocomposites obtained from cation-exchanged zeolite by heat treatment in reducing atmosphere. Microporous Mesoporous Mater. 268, 131-143. https://doi.org/10.1016/j.micromeso.2018.04.024 .

Esposito S., Marocco A., Bonelli B., Pansini M., PCT international application published under Number WO**2015**/145230 A1.

Esposito S., Marocco A., Bonelli B., Pansini M., Produzione di Materiali Compositi Metallo-Ceramici Nano Strutturati da Precursori Zeolitici. Brevetto Italiano, MI**2014**A000522.

Esposito S., Marocco A., Dell'Agli G., Bonelli B., Mannu F., Allia P., Tiberto P., Barrera G., Pansini M., 2020. Separation of biological entities from human blood by using magnetic nanocomposites obtained from zeolite precursors. Molecules 25, 1803-1821. https://doi.org/10.3390/molecules25081803 .

Esposito S., Sannino F., Pansini M., Bonelli B., Garrone E., 2013. Modes of interaction of simazine with the surface of model amorphous silicas in water. J. Phys. Chem. C 117, 11203-11210. https://doi.org/10.1021/jp401997s.

Freyria F.S., Marocco A., Esposito S., Bonelli B., Barrera G., Tiberto P., Allia P., Oudayer P., Roggero A., Matéo-Vélez J.C., Dantras E., Pansini M., 2019. Simulated Moon agglutinates obtained from zeolite precursor by means of a low-cost and scalable synthesis method. ACS Earth Sp. Chem. 3, 1884-1895. https://doi.org/10.1021/acsearthspacechem.9b00042.

Fukahori S., Fujiwara T., Funamizu N., Matsukawa K., Ito R., 2013. Adsorptive removal of sulfonamide antibiotics in livestock urine using the high-silica zeolite HSZ-385. Water Sci Technol. 67, 319-325. https://doi.org/10.2166/wst.2012.513.

Giles A., Jaime Foushee, Evan Lantz and Giuseppe Gumina 2019. Sulfonamide Allergies. Pharmacy, 132, 1-12. https://doi:10.3390/pharmacy7030132.

Guo F.Q., Li X.L., Jiang X.C., Zhao X.M., Guo C.L., Rao Z.H., 2018. Characteristics and toxic dye adsorption of magnetic activated carbon prepared from biomass waste by modified one-step synthesis. Colloids Surf A Physicochem Eng Asp 555, 43-54.

Kassinos D.F., Meric S., Nikolaou A., 2011. Pharmaceutical residues in environmental waters and wastwater: current state of knowledge and future research. Anal. Bioanal. Chem. 399, 251-275. https://doi.org/10.1007/s00216-010-4300-9.

Kochuk EV, Dmitrienko SG (2011) Sorption of sulfanilamides on highly crosslinked polystyrene. Russ J Phys Chem A 85:89–93

Korzh EA, Smolin SK, Klymenko NA (2016) Impact of characteristic of activated carbons on the efficiency of removal from water of pharmaceutical preparations of various chemical nature. J Water Chem Technol 38:83–88

Langella, A.; Pansini, M.; Cerri, G.; Cappelletti, P.; de'Gennaro M., 2003. Thermal behaviour of natural and cation-exchanged clinoptilolite from Sardinia (Italy). Clays and Clay Minerals 51, 625-633.

Manzoli M., Tammaro O., Marocco A., Bonelli B., Barrera G., Tiberto P., Allia P., Matéo-Vélez J.C., Roggero A., Dantras E., Arletti R., Pansini M., Esposito S., 2021. New insights in the

production of simulated moon agglutinates: the use of natural zeolite-bearing rocks. ACS Earth Space Chem. 5, 1631-1646. https://doi.org/10.1021/acsearthspacechem.1c00118 .

Marocco A., Dell'Agli G., Esposito S., Pansini M., 2012. Metal-ceramic composite materials from zeolite precursor. Sol. St. Sc. 14, 394-400. https://doi.org/10.1016/j.solidstatesciences.2012.01.006 .

Marocco A., Dell'Agli G., Sannino F., Esposito S., Bonelli B., Allia P., Tiberto P., Barrera G., Pansini M., 2020. Removal of agrochemicals from waters by adsorption: a critical comparison among humic-like substances, zeolites, porous oxides, and magnetic nanocomposites. Processes 8, 141-167. https://doi.org/10.3390/pr8020141.

Marocco A., Liguori B., Dell'Agli G., Pansini M., 2011. Sintering behaviour of celsian based ceramics obtained from the thermal conversion of (Ba, Sr)-exchanged zeolite A. J. Eur. Ceram. Soc. 31, 1965-1973. https://doi.org/10.1016/j.jeurceramsoc.2011.04.028 .

Martucci, A., Braschi, I., Marchese, L., Quartieri, S., 2014. Recent advances in clean-up strategies of waters polluted with sulfonamide antibiotics: a review of sorbents and related properties. Min. Mag.,78, 1115-1140.

Mendiola-Alvarez, S.Y., Turnes-Palomino, G., Guzm ´ an-Mar, J., Hern ´ andez-Ramírez, A., Hinojosa-Reyes, L., Palomino-Cabello, C., 2020. Magnetic porous carbons derived from cobalt(II)-based metal – organic frameworks for the solid phase extraction of sulfonamides. Dalton Trans. 49, 8959. https://doi.org/10.1039/d0dt01215g.

Neu H.C., Gootz T.D., Antimicrobial chemotherapy, in: S. Baron, (Ed.), Medical Microbiology, fourth ed., University of Texas Medical Branch at Galveston, Galveston (TX), 1996.

Ortiz I., Mosquera-Corral A., Rodicio J.L., Esplugas S., 2015. Advanced technologies for water treatment and reuse. AIChE J. 61, 3146-3158. https://doi.org/10.1002/aic.15013.

Ozacar M., Sengil I.A., 2006. A two stage batch adsorber design for methylene blue removal to minimize contact time. J. Environ. Manag. 80, 372-379. https://doi.org/10.1016/j.jenvman.2005.10.004 .

Pansini M., Colella C., 1990. Dynamic data on lead uptake from water by chabazite. Desalination 78, 287-295. https://doi.org/10.1016/0011-9164(90)80048-G .

Pansini M., De Gennaro R., Parlato L., De'Gennaro M., Langella A., Marocco A., Cappelletti P., Mercurio M., 2010. Use of sawing waste from zeolitic tuffs in the manufacture of ceramics. Adv. Mater. Sci. Eng. 2010, 1-9. https://doi.org/10.1155/2010/820541 .

Pansini M., Dell'Agli G., Marocco A., Netti P.A., Battista E., Lettera V., Vergara P., Allia P., Bonelli B., Tiberto P., Barrera G., Alberto G., Martra G., Arletti R., Esposito S., 2017. Preparation and charaterization of magnetic and porous metal-ceramic nanocomposites from a

zeolite precursor and their application for DNA separation. J. Biomed. Nanotechnol. 13, 337-348. https://doi.org/10.1166/jbn.2017.2345 .

Pansini M., Sannino F., Marocco A., Allia P., Tiberto P., Barrera G., Polisi M., Battista E., Netti P.A., Esposito S., 2018. Novel process to prepare magnetic metal-ceramic nanocomposites from zeolite precursor and their use as adsorbent of agrochemicals from water. J. Environ. Chem. Eng. 6, 527-538. https://doi.org/10.1016/j.jece.2017.12.030 .

Pirozzi D., Imparato C., D'Errico G., Vitiello G., Aronne A., Sannino F., 2020. Three-year lifetime and regeneration of superoxide radicals on the surface of hybrid TiO_2 materials exposed to air. Journal of Hazardous Materials 387, 121716. https://doi.org/10.1016/j.jhazmat.2019.121716

Qin L.T., Pang X.R., Zeng H.H., Liang Y.P., Mo L.Y., Wang D.Q., Dai J.F., 2020. Ecological and human health risk of sulfonamides in surface water and groundwater of Huixian karst wetland in Guilin, China. Sci. Total Environ. 708, 134552-134561. https://doi.org/10.1016/j.scitotenv.2019.134552.

Rashed M.N., 2013. Adsorption Technique for the Removal of Organic Pollutants from Water and Wastewater, Organic Pollutants - Monitoring, Risk and Treatment, M. Nageeb Rashed, IntechOpen, DOI: 10.5772/54048.

Ronchetti S., Turcato E.A., Delmastro A., Esposito S., Ferone C., Pansini M., Onida B., D. Mazza, 2010. Study of the thermal transformations of Co- and Fe- exchanged zeolites A and X by "in situ" XRD under reducing atmosphere. Mater. Res. Bull. 45, 744-750. https://doi.org/10.1016/j.materresbull.2010.02.006 .

Sabri N.A., Schmitt H., Van der Zaan B., Gerritsen H.W., Zuidema T., Rijnaarts H.H.M., Langenhoff A.A.M., 2020. Prevalence of antibiotics and antibiotic resistance genes in a wastewater effluent-receiving river in the Netherlands. J. Environ. Chem. Eng. 8. 102245-102256. https://doi.org/10.1016/j.jece.2018.03.004 .

Sannino F., Pernice P., Minieri L., Camandona G.A., Aronne A., Pirozzi D., 2015. Oxidative Degradation of Different Chlorinated Phenoxyalkanoic Acid Herbicides by a Hybrid ZrO2 Gel-Derived Catalyst without Light Irradiation. ACS Applied Materials & Interfaces *7* (1), 256-263. https://pubs.acs.org/doi/10.1021/am506031e

Sannino F., Pirozzi D., Vitiello G., D'Errico G., Aronne A., Fanelli E., Pernice P., 2014. Oxidative degradation of phenanthrene in the absence of light irradiatiion by hybrid ZrO2-acetylacetonate gel-derived catalyst. Applied Catalysis B: Environmental 156–157, 101-107. https://doi.org/10.1016/j.apcatb.2014.03.006

Sannino F., Ruocco S., Marocco A., Esposito S., Pansini M., 2012. Cyclic process of simazine removal from waters by adsorption on zeolite HY and its regeneration by thermal treatment. J. Hazard. Mat. 229-230, 354-360. https://doi.org/10.1016/j.jhazmat.2012.06.011 .

Sannino F., Ruocco S., Marocco A., Esposito S., Pansini M., 2013a. Simazine removal from waters by adsorption on porous silicas tailored by sol–gel technique. Microporous and Mesoporous Materials 180, 178-186. https://doi.org/10.1016/j.micromeso.2013.06.026

Sannino F., Ruocco S., Marocco A., Esposito S., Pansini M., 2013b. Simazine removal from waters by adsorption on porous silicas tailored by sol–gel technique. Microporous Mesoporous. Mater., 180, 178-186. https://doi.org/10.1016/j.micromeso.2013.06.026 .

Shi P, Ye N (2015) Investigation of the adsorption mechanism and preconcentration of sulfonamides using a porphyrin-functionalized Fe_3O_4-graphene oxide nanocomposite. Talanta 143:219–225

Sköld O., 2000. Sulfonamide resistance: mechanisms and trends, Drug Resistance Updates, 3(3), 155-160, https://doi.org/10.1054/drup.2000.0146.

Sousa, D.N.R., Insa, S., Mozeto, A.A., Petrovic, M., Chaves, T.F., Fadini, P.S., 2018. Equilibrium and kinetic studies of the adsorption of antibiotics from aqueous solutions onto powdered zeolites. Chemosphere 205, 137–146.

Srivastava B., Jhelum V., Basu D.D., Patanjali P.K., 2009. Adsorbents for pesticide uptake from contaminated water: A review, J. Sci. Ind. Res 68, 839-850. http://nopr.niscair.res.in/handle/123456789/6128 .

Tilles SA. (2001) Practical issues in the management of hypersensitivity reactions: sulfonamides. South Med J., 94(8):817-24.

Uhlemann T., Berden G., Oomens J., 2021. Preferred protonation site of a series of sulfa drugs in the gas phase revealed by IR spectroscopy. Eur. Phys. J. D 75, 1-13. https://doi.org/10.1140/epjd/s10053-020-00027-x .

van Mil, The Complete Drug Reference, Sweetman S. (Ed.). The Pharmaceutical Press, London, 2011.

Wan J., Ding J., Tan W., Gao Y., Sun S., He C., 2020. Magnetic-activated carbon composites derived from iron sludge and biological sludge for sulfonamide antibiotic removal. Environ. Sci. Poll. Res. 27, 13436-13446. https://doi.org/10.1007/s11356-020-07940-z.

Yang, C.W., Hsiao, W.C., Chang, B.V., 2016. Biodegradation of sulfonamide antibiotics in sludge. Chemosphere 150, 559 – 565. https://doi.org/10.1016/j.

Zhou Y., Meng J., Zhang M., Chen S., He B., Zhao H., Li Q., Zhang S., Wang T., 2019. Which type of pollutants need to be controlled with priority in wastewater treatment plants: Traditional or

emerging pollutants?. Environ. Int. 131, 104982-104995. https://doi.org/10.1016/j.envint.2019.104982 .

Captions for Figures

Figure 1 – Effect of pH on the adsorption of sulfanilamide on ZA1, ZA2 and LB1 magnetic adsorbents. S/L ratio = 1/10000, contact time = 24 h

Figure 2 – (a) Ionization scheme of sulfanilamide (figure taken from http://www.organicchem.org) (b) speciation of sulfanilamide as a function of pH (figure taken from Dai et al., 2017)

Figure 3 - ζ-potential curve of samples ZA1, ZA2 and LB1, in deionized water at room temperature.

Figure 4 – Adsorption kinetics of sulfanilamide uptake:
(a) in the presence of ZA1 and LB1 magnetic adsorbents (S/L ratio = 1/10,000, pH 6.0 and 4.0, initial sulfanilamide concentration = 40.0 μmol/L).
(b) in the presence of LB1 magnetic adsorbent (S/L ratio = 1/10,000, pH 4.0, initial sulfanilamide concentrations of 40.0 and 126 μmol/L).

Figure 5 – Adsorption isotherms of sulphanilamide on ZA1 and LB1 magnetic adsorbents.

Figure 6 – DTA curve (a) and TG curve (b) of sulfanilamide

Figure 7 – Adsorption capacity the adsorbents ZA1 and LB1 regenerated by alkaline treatment, after each desorption/adsorption cycle

Figure 1.

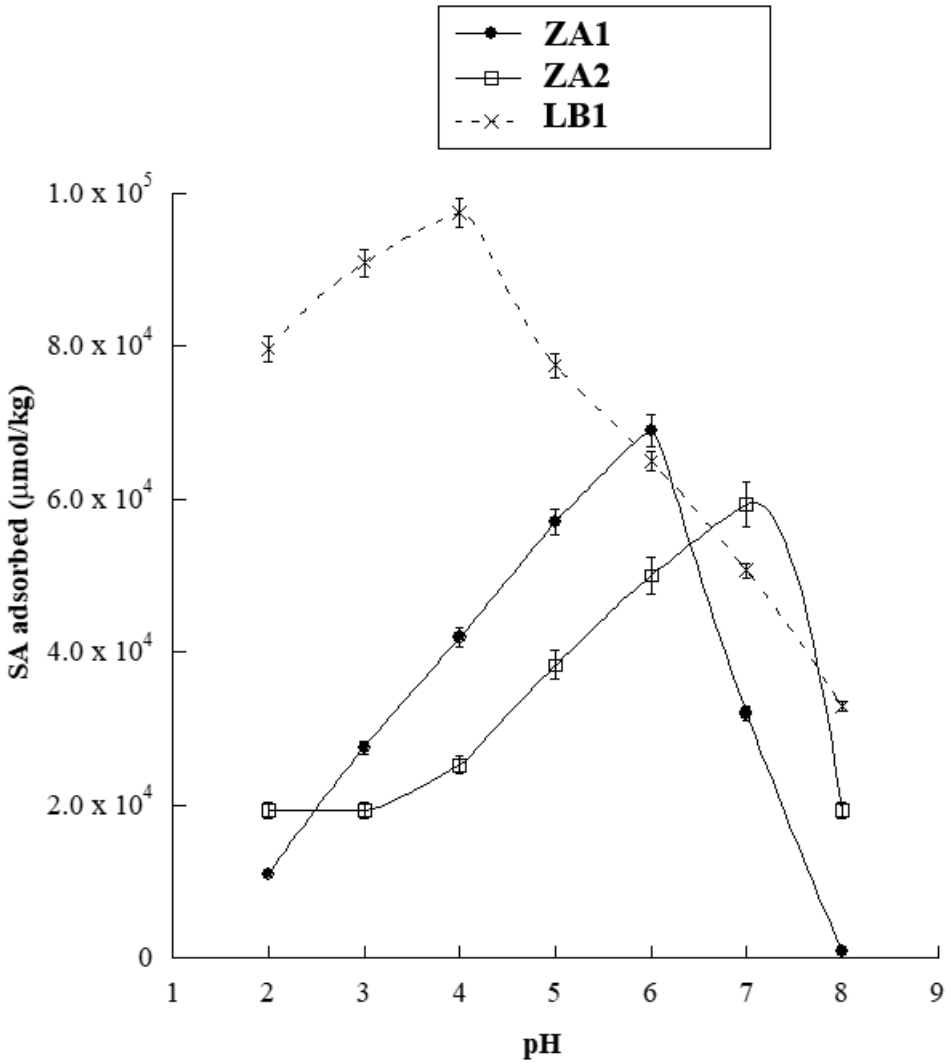
ZA1
ZA2
LB1
1.0 x 10^5
8.0 x 10^4
6.0 x 10^4
4.0 x 10^4
2.0 x 10^4
0
SA adsorbed (μmol/kg)
1
2
3
4
5
6
7
8
9
pH

Figure 2

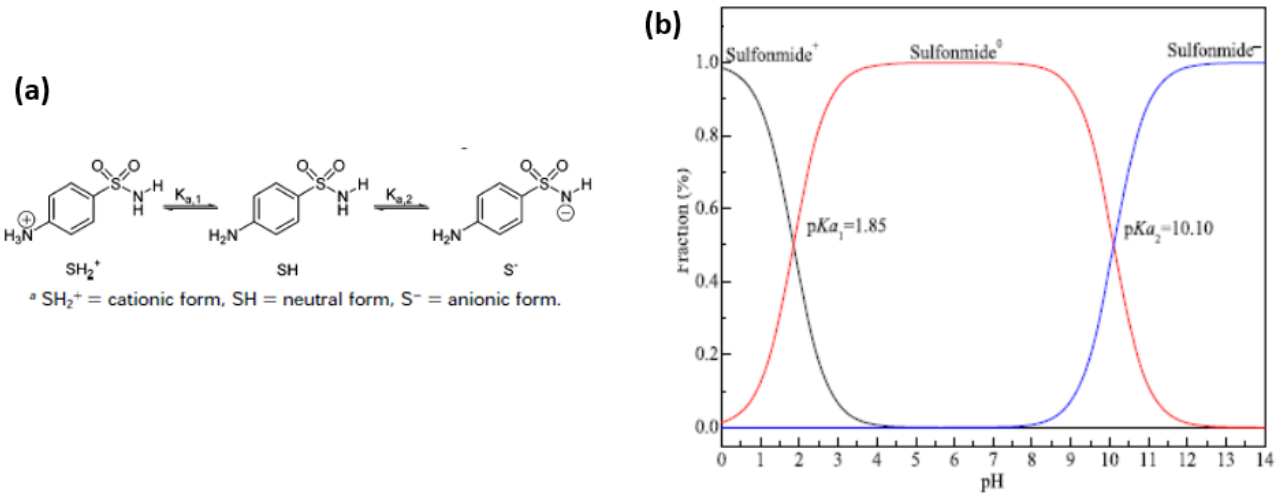
(a)
$K_{a,1}$
$K_{a,2}$
SH_2^+
SH
S^-
[a] SH_2^+ = cationic form, SH = neutral form, S^- = anionic form.
(b)
Sulfonmide$^+$
Sulfonmide^0
Sulfonmide$^-$
pKa_1=1.85
pKa_2=10.10
Fraction (%)
pH

Figure 3

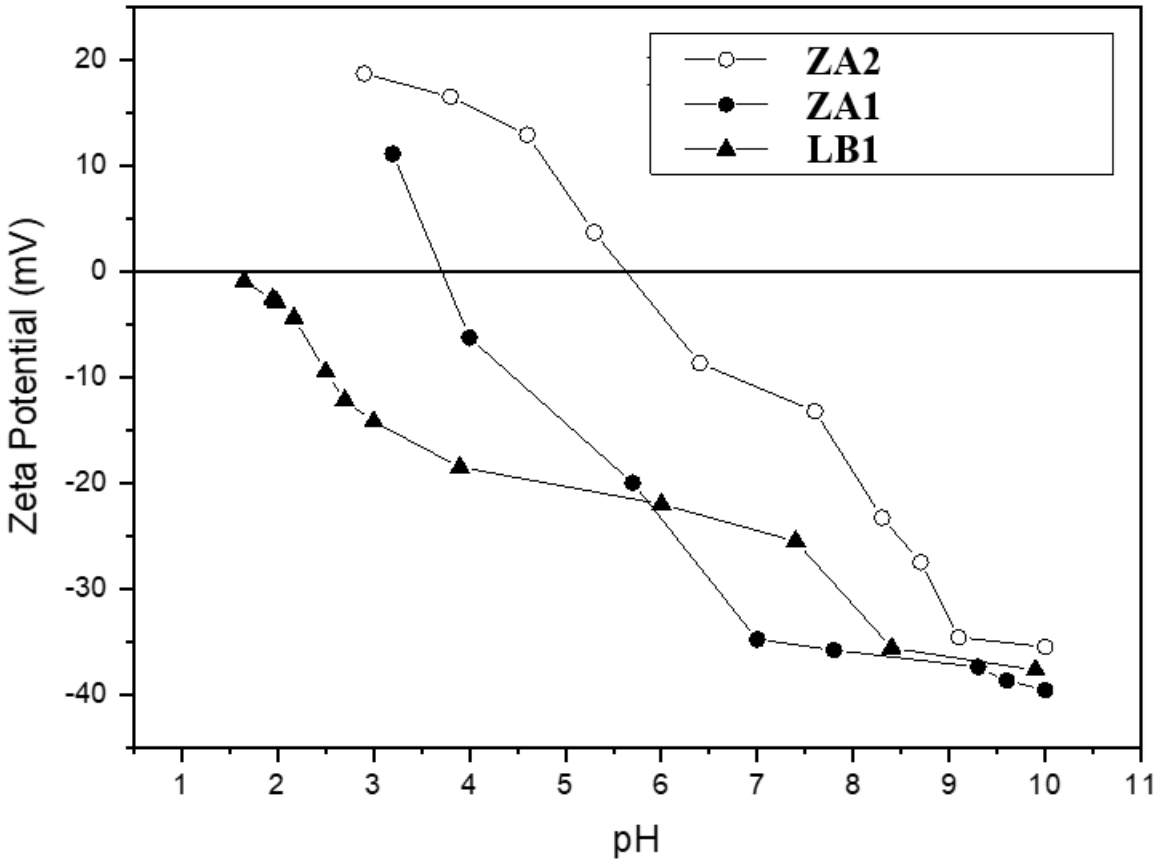
ZA2
ZA1
LB1
Zeta Potential (mV)
pH
20
10
0
-10
-20
-30
-40
1
2
3
4
5
6
7
8
9
10
11

Figure 4a.

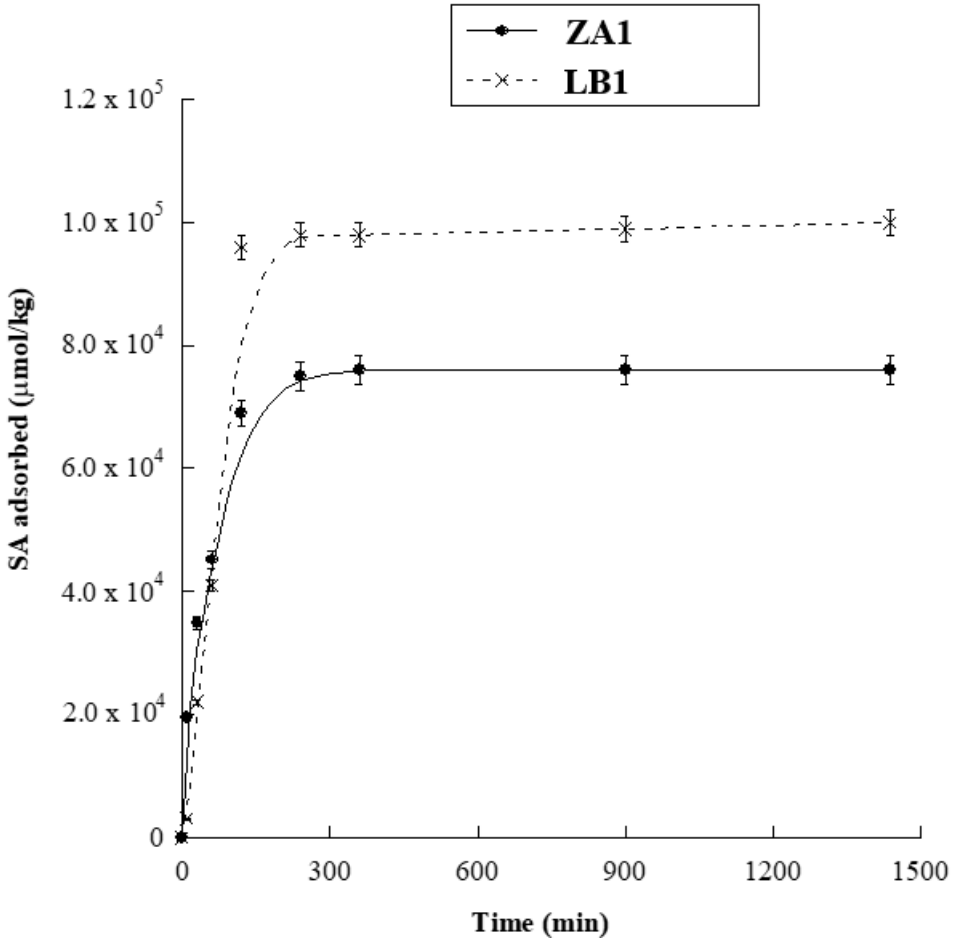
ZA1
LB1
1.2 x 10^5
1.0 x 10^5
8.0 x 10^4
6.0 x 10^4
4.0 x 10^4
2.0 x 10^4
0
SA adsorbed (μmol/kg)
0
300
600
900
1200
1500
Time (min)

Figure 4b.

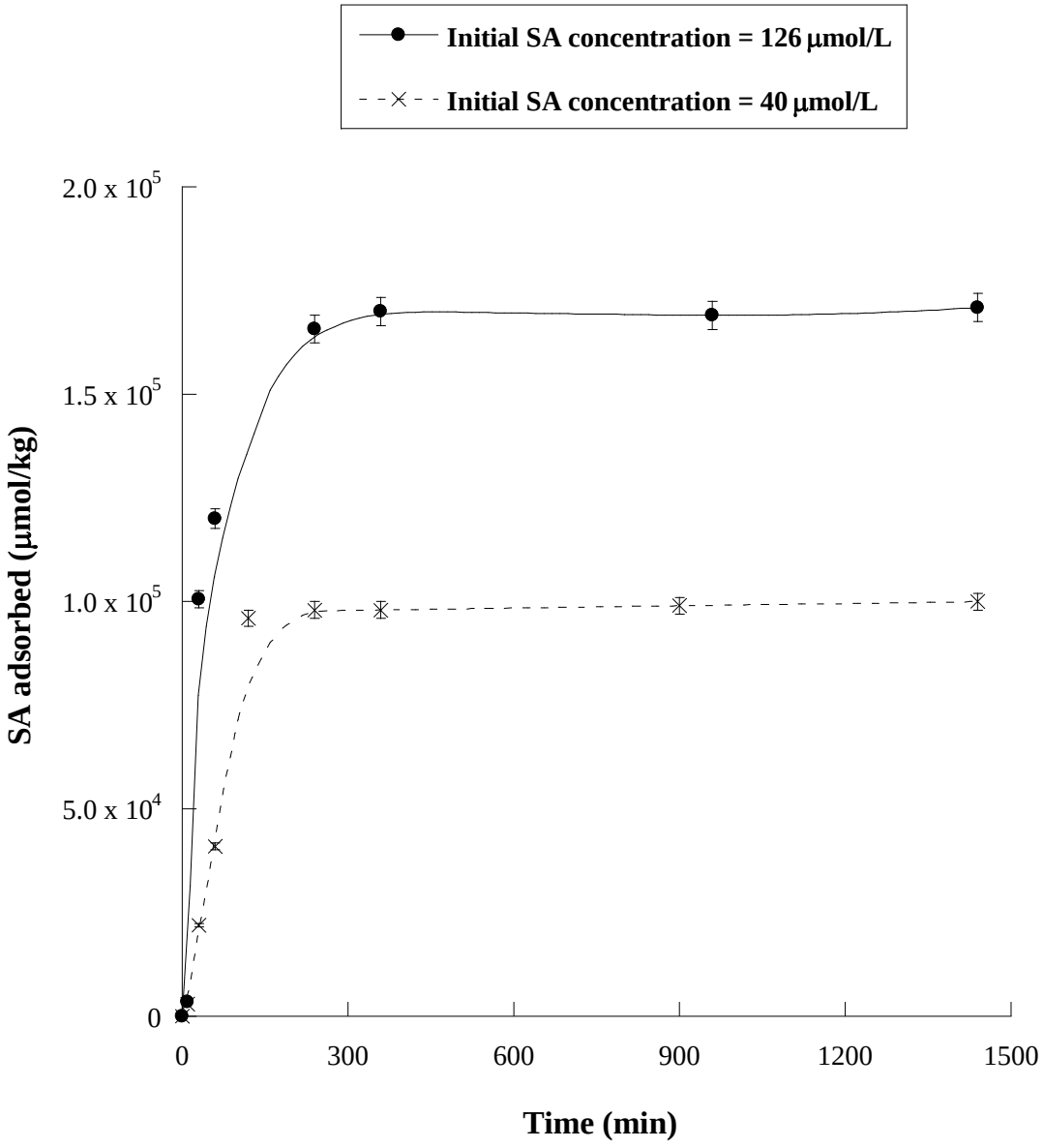
Initial SA concentration = 126 μmol/L
Initial SA concentration = 40 μmol/L
2.0 x 10^5
1.5 x 10^5
1.0 x 10^5
5.0 x 10^4
0
SA adsorbed (μmol/kg)
0
300
600
900
1200
1500
Time (min)

Figure 5.

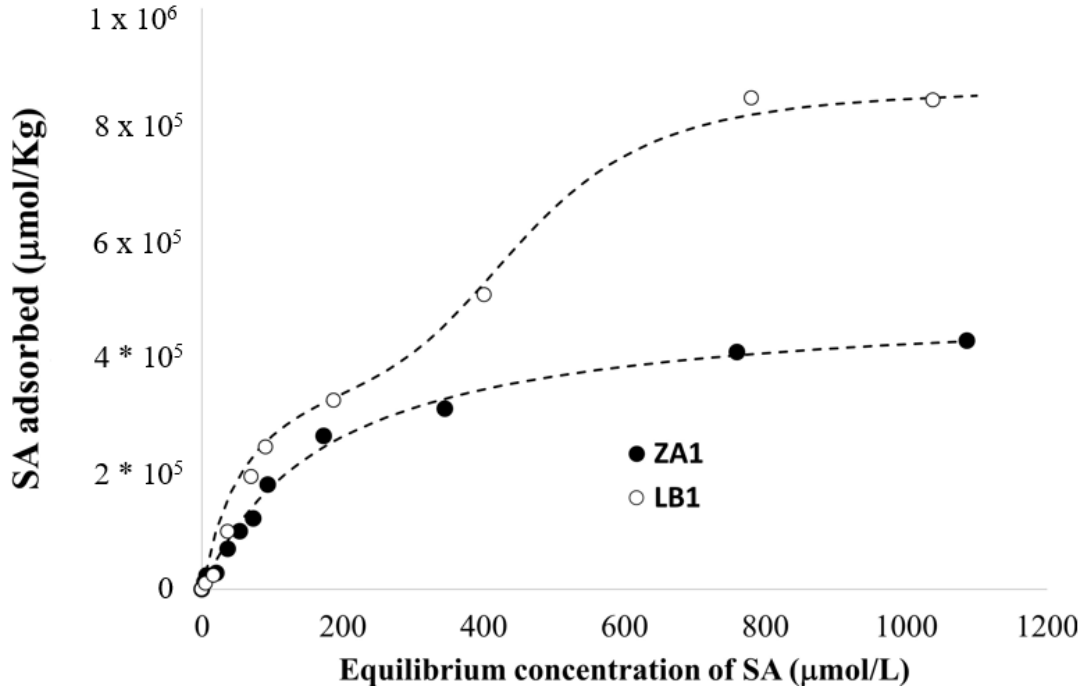
1 x 10^6
8 x 10^5
6 x 10^5
4 * 10^5
2 * 10^5
0
SA adsorbed (µmol/Kg)
0
200
400
600
800
1000
1200
Equilibrium concentration of SA (µmol/L)
ZA1
LB1

Figure 6a.

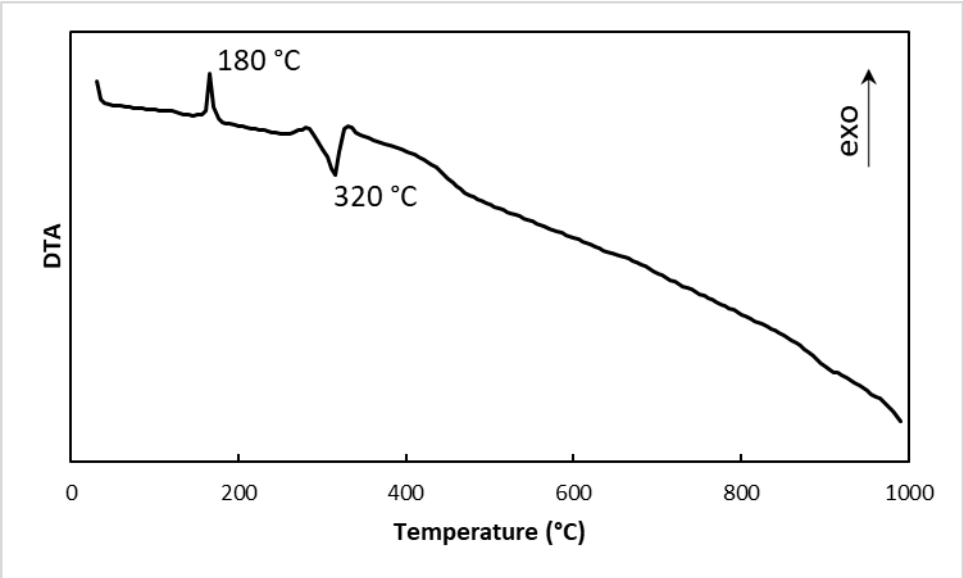

Figure 6b.

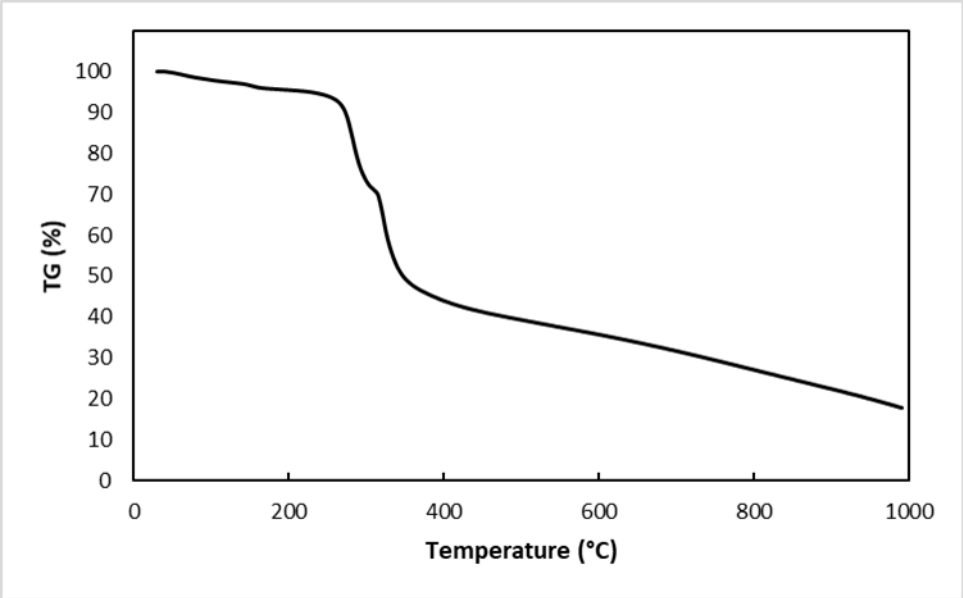

Figure 7.

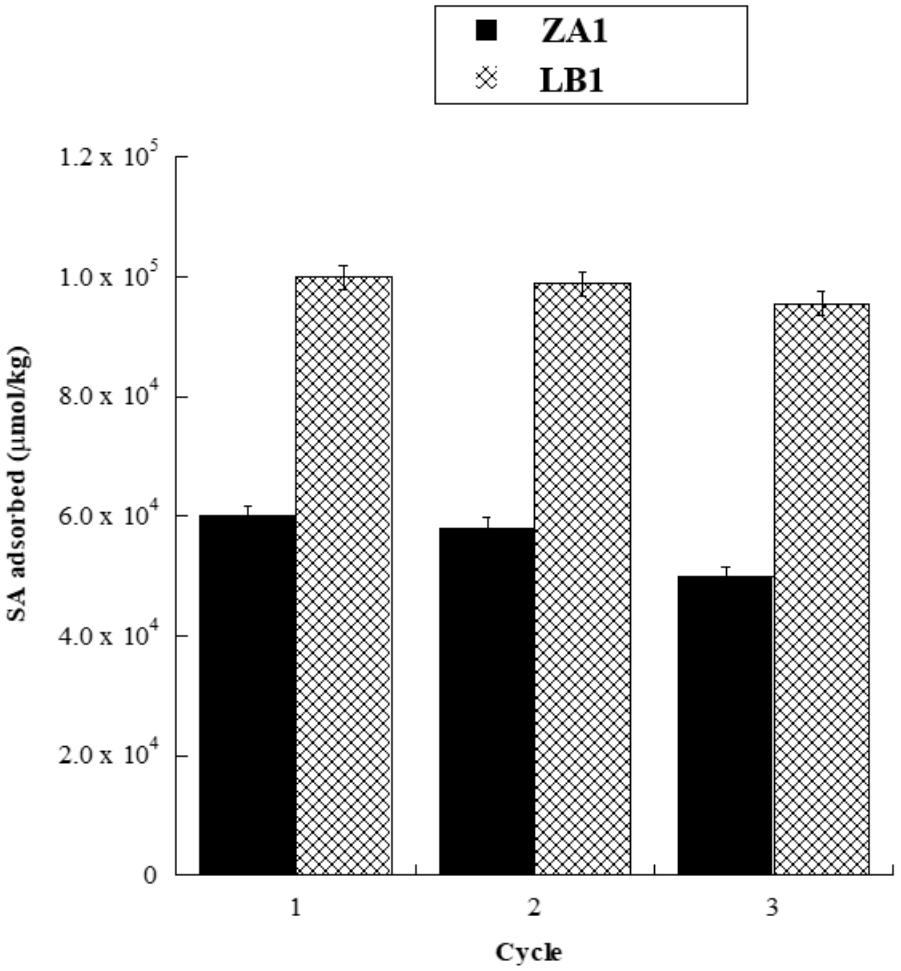
ZA1
LB1
1.2 x 10^5
1.0 x 10^5
8.0 x 10^4
6.0 x 10^4
4.0 x 10^4
2.0 x 10^4
0
SA adsorbed (µmol/kg)
1
2
3
Cycle